PHYSICAL REVIEW B **95**, 235114 (2017)

Determination of Hund's coupling in 5*d* oxides using resonant inelastic x-ray scattering

Bo Yuan,[1] J. P. Clancy,[1] A. M. Cook,[1,2] C. M. Thompson,[3,*] J. Greedan,[3,4] G. Cao,[5] B. C. Jeon,[6,7] T. W. Noh,[6,7] M. H. Upton,[8]
D. Casa,[8] T. Gog,[8] A. Paramekanti,[1] and Young-June Kim[1,†]
[1]*Department of Physics, University of Toronto, Toronto, Ontario, Canada M5S 1A7*
[2]*Department of Physics, University of Zurich, Winterthurerstrasse 190, 8057 Zurich, Switzerland*
[3]*Department of Chemistry and Chemical Biology, McMaster University, Hamilton, Ontario, Canada L8S 4L8*
[4]*Brockhouse Institute for Materials Research, McMaster University, Hamilton, Ontario, Canada L8S 4L8*
[5]*Department of Physics, University of Colorado Boulder, Boulder, Colorado 80309, USA*
[6]*Center for Correlated Electron Systems, Institute for Basic Science, Seoul 08826, Republic of Korea*
[7]*Department of Physics and Astronomy, Seoul National University, Seoul 08826, Republic of Korea*
[8]*XSD, Advanced Photon Source, Argonne National Laboratory, Argonne, Illinois 60439, USA*

(Received 23 January 2017; published 8 June 2017)

We report resonant inelastic x-ray scattering (RIXS) measurements on ordered double-perovskite samples containing Re^{5+} and Ir^{5+} with $5d^2$ and $5d^4$ electronic configurations, respectively. In particular, the observed RIXS spectra of $\mathrm{Ba_2YReO_6}$ and $\mathrm{Sr_2}M\mathrm{IrO_6}$ (M = Y, Gd) show sharp intra-t_{2g} transitions, which can be quantitatively understood using a minimal "atomic" Hamiltonian incorporating spin-orbit coupling λ and Hund's coupling J_H. Our analysis yields $\lambda = 0.38(2)$ eV with $J_H = 0.26(2)$ eV for Re^{5+} and $\lambda = 0.42(2)$ eV with $J_H = 0.25(4)$ eV for Ir^{5+}. Our results provide sharp estimates for Hund's coupling in 5*d* oxides and suggest that it should be treated on equal footing with spin-orbit interaction in multiorbital 5*d* transition-metal compounds.

DOI: 10.1103/PhysRevB.95.235114

I. INTRODUCTION

Hund's coupling J_H represents the local spin-exchange interaction for electrons in multiorbital systems, and it is responsible for a variety of interesting phenomena in solids. For example, Hund's coupling is responsible for spin-state transitions as a function of temperature in certain insulating 3*d* transition-metal compounds [1–5]. More remarkably, Hund's coupling has two distinct and contrary effects in multiband metals [6]. On the one hand, it suppresses the atomic charge gap, making it energetically unfavorable for electrons to be localized and become a Mott insulator. On the other hand, it promotes strongly correlated bad-metal behavior by rendering Fermi-liquid quasiparticles incoherent. This dichotomous role played by J_H is now recognized to be important in the widely studied iron pnictides [7–13], as well as in ruthenates like $\mathrm{Ca_2RuO_4}$ [14,15].

In recent years, there has been increasing interest in complex 5*d* oxides. In these systems, there is an intricate interplay of electronic correlation, Hund's coupling, spin-orbit coupling (SOC) λ, and electron kinetic energy, which leads to novel ground states [16]. This underscores the need to accurately determine these energy scales, which has important ramifications for magnetism, bad-metal behavior, and Mott transitions in 5*d* oxides. For example, density-functional-theory calculations predict the honeycomb material $\mathrm{(Na,Li)_2IrO_3}$ to exhibit a large bandwidth and weakly correlated behavior [17,18]. However, experiments show that it is better described as a $J_{\mathrm{eff}} = 1/2$ Mott insulator [19–21], in agreement with a recent exact diagonalization study which accounts for local correlation effects [22]. Similarly, d^4 systems with strong SOC have been predicted to behave as localized $J_{\mathrm{eff}} = 0$ insulators, with magnetism induced by exciton condensation [23–26] or impurity effects [27], while band theory [28] provides an itinerant magnetism explanation for the observed Ir magnetic moment in $A_2\mathrm{YIrO_6}$ (A = Ba,Sr) [27,29]. Incorporation of correlation effects appears to be necessary to resolve the controversy in understanding magnetism in d^4 double perovskites. The interplay of SOC and Hund's coupling is also clearly important in understanding the electronic ground states in multielectron $5d^2$ rhenates and $5d^3$ osmates [30,31]. While Hund's coupling is irrelevant for the single-hole atomic configuration of Mott-insulating $5d^5$ iridates, it is important for superexchange processes which involve intermediate $5d^4$ configurations (two-hole states). This determines the strength of the conventional Heisenberg interaction relative to the unconventional Kitaev exchange which can drive an exotic quantum spin liquid in honeycomb-based materials [20,21,32–40].

Remarkably, despite this wide interest in complex 5*d* oxides and the importance of Hund's coupling for understanding their magnetic properties, there has been no direct and accurate experimental determination of J_H in these systems. The values for J_H used in numerical calculations on 5*d* oxides vary widely, ranging from $J_H = 0.2$ to 0.6 eV [18,22,27,41,42], while analytical studies typically focus on the simple limits $J_H \gg \lambda$ or $J_H \ll \lambda$.

In this paper, we use resonant inelastic x-ray scattering (RIXS) to explore local spin-orbital excitations in Ir^{5+} ($5d^4$) and Re^{5+} ($5d^2$) double perovskites. Use of the two complementary 5*d* insulating oxides modeled by an effective "atomic" Hamiltonian allows us to determine these important energy scales, J_H and λ, with high precision. We find $\lambda(\mathrm{Ir}) = 0.42(2)$ eV with $J_H(\mathrm{Ir}) = 0.25(4)$ eV and $\lambda(\mathrm{Re}) = 0.38(2)$ eV with $J_H(\mathrm{Re}) = 0.26(2)$ eV. The J_H values obtained here represent the first measurements for rhenates and iridates.

---

[*] Present address: Department of Chemistry, Purdue University, 560 Oval Drive, West Lafayette, Indiana 47907-2084, USA.

[†] yjkim@physics.utoronto.ca

II. EXPERIMENTAL METHODS

In our study, we choose to work with ordered double-perovskite (DP) compounds $A_2BB'O_6$ (B = Ir, Re), which offer two distinct advantages. In Ba_2YReO_6 and Sr_2YIrO_6, the Re/Ir octahedra form a rock-salt structure with adjacent octahedra centered around inert Y^{3+} ions. The intervening electronically inactive YO_6 octahedra ensures that the overlap between the neighboring Re/Ir orbitals is small, leading to extremely narrow spectral bandwidths, as shown in our RIXS data. This allows us to focus on the local physics and justifies our use of an atomic Hamiltonian to model the data. The second benefit of using DPs has to do with suppression of the Jahn-Teller (J-T) instability. In a perovskite structure with octahedra formed by d^2 or d^4 ions, there is a tendency for a cooperative J-T effect, in which neighboring octahedra distort in a complementary manner which strongly breaks the local octahedral symmetry. However, if the J-T active octahedron is surrounded by octahedra containing non-J-T ions (such as Fe^{3+} or Y^{3+}), this instability is suppressed [43]. As a result, although the ReO_6 and IrO_6 octahedra in the DP structure may undergo small rotations, they lead to very weak deviations from an ideal local octahedral environment.

Two different experimental setups were used for the RIXS experiments at the Advanced Photon Source. For the Ir L_3 (Re L_2) edge RIXS experiments carried out at the 9ID (27ID) beamline, the beam was monochromatized by Si(844) [Si(400)] crystals. A spherical (1-m-radius) diced Si(844) [Si(773)] analyzer was used to select final photon energy. In order to minimize the elastic background intensity, measurements were carried out in a horizontal scattering geometry, for which the scattering angle 2θ was close to 90°. An overall energy resolution of about 40 meV (FWHM) for Ir and 100 meV for Re was obtained. The Re-DP samples used in our measurements, Ba_2YReO_6, Ba_2FeReO_6, and Ca_2FeReO_6, were all polycrystalline powder samples pressed into pellets. For Ir-DP measurements, we used single crystals of Sr_2YIrO_6 and Sr_2GdIrO_6. The synthesis and characterization of these samples have been previously reported [29,43–47], and all samples show a high degree of B/B' order due to the valence difference.

III. EXPERIMENTAL RESULTS

The incident energy E_i dependence of Ba_2YReO_6 RIXS spectra is shown in Fig. 1. One can resolve three main features with $\hbar\omega \lesssim 2.5$ eV (feature A), $4\,\text{eV} \lesssim \hbar\omega \lesssim 6$ eV (feature B), and $6\text{eV} \lesssim \hbar\omega \lesssim 8$ eV (feature C). Both features A and C show enhancement when E_i is tuned near the resonance energy of $E_i \approx 11.961$ keV, whereas feature B resonates at slightly higher $E_i \approx 11.965$ keV. RIXS follows a second-order process (dipole transition from $2p$ to $5d$ and another transition back to $2p$) with an intermediate state consisting of a $2p$ core hole and an excited electron in either t_{2g} or e_g states. Different resonant energies thus reflect different intermediate states in these transitions. This allows us to assign A and C as intra-t_{2g} and charge-transfer (CT) excitation from the surrounding ligands to t_{2g} states, respectively, and B as a t_{2g}-e_g transition. The intermediate states of both intra-t_{2g} and CT excitation are $\underline{2p}t_{2g}^3$, where the underline denotes a $2p$ core hole. On the other hand, the intermediate state for the t_{2g}-e_g transition is $\underline{2p}t_{2g}^2e_g^1$, which occurs at higher energy than $\underline{2p}t_{2g}^3$. The difference in resonant energies thus corresponds to the t_{2g}-e_g splitting. As discussed earlier, the spatial extent of the $5d$ orbital leads to a large t_{2g}-e_g splitting, while the t_{2g} orbitals are further split by J_H and λ, as shown in Fig. 1. We note that strong fluorescence features were observed around 10 eV in the study of metallic rhenate samples ReO_2 and ReO_3 [48], which is absent in our E_i-dependence study of insulating Ba_2YReO_6. A qualitatively similar incident energy dependence has been reported for iridate samples in the past [49].

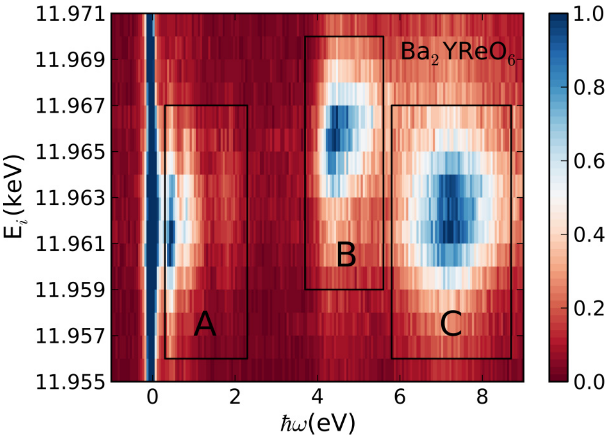

FIG. 1. Incident energy E_i dependence of Ba_2YReO_6 RIXS spectra. The RIXS intensity is plotted as a function of incident energy E_i (vertical axis) and energy transfer $\hbar\omega$ (horizontal axis). An arbitrary intensity scale is used, where blue (red) denotes higher (lower) intensity.

Room-temperature RIXS spectra of all DP samples are shown in Fig. 2. Wide-range scans are shown in the insets of Figs. 2(a) and 2(b) for Ir DPs and Re DPs, respectively. The low-energy region below 2.5 eV is zoomed in on and shown in the main panels. All samples are found to exhibit qualitatively similar excitation spectra: a set of sharp peaks in the low-energy range $\lesssim$2.5 eV (the sharp $\hbar\omega = 0$ peaks are due to the elastic background and represent instrumental resolution) and two broader peaks in the high energy 4–8 eV range. Despite the similarity in the peak positions, we find a systematic difference in the peak widths when comparing different samples. In particular, metallic Ba_2FeReO_6 and semimetallic Ca_2FeReO_6 exhibit very broad features, clearly contrasting the other (insulating) samples, which exhibit well-resolved peaks. We thus focus below on the spectra of only the insulating samples in order to extract quantitative information from the peak positions.

As shown in Fig. 2(a), the Ir-DP samples display sharp features that are resolution limited. The three inelastic peak positions in both Sr_2GdIrO_6 and Sr_2YIrO_6 can be read directly from their spectra: 0.39(2), 0.66(2), and 1.30(6) eV. No momentum dependence was found for these features (see Appendix B). In addition, there is a very weak feature at ~2 eV in both iridates. We note that the crystal structures of these two compounds are different; Sr_2YIrO_6 and Sr_2GdIrO_6 crystallize in monoclinic and cubic symmetry, respectively [29]. In addition, the IrO_6 octahedra are slightly flattened

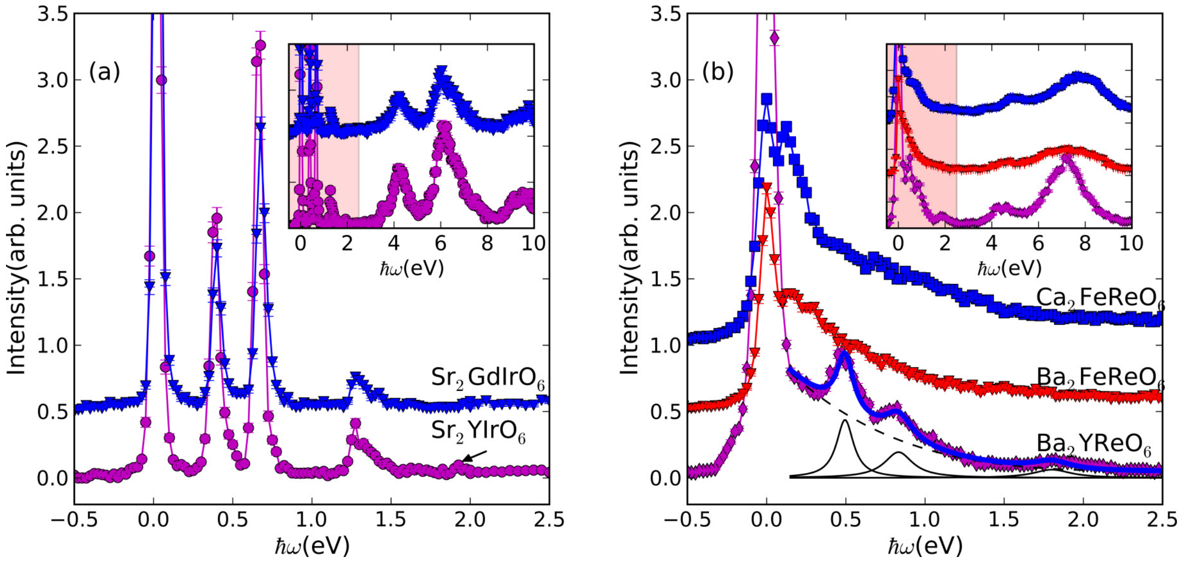

FIG. 2. RIXS spectra of (a) Ir double perovskites and (b) Re double perovskites. Main panels show details of intra-t_{2g} excitations in the energy range $\hbar\omega < 2.5$ eV, while full RIXS spectra covering a wide range of energy transfer $\hbar\omega < 10$ eV are shown in the insets. Incident energies $E_i = 11.215$ keV and $E_i = 11.961$ keV with fixed Q near $2\theta = 90^\circ$ were used to obtain spectra in (a) and (b), respectively. The scans are vertically offset for visual clarity, and the intensity scale is arbitrary. The arrow in (a) indicates the weak ~2 eV feature (see text). The thick blue line in (b) is a fit to the Ba$_2$YReO$_6$ spectrum as described in the text. Contributions from individual peaks are shown as black solid lines. The dashed line indicates the sloping quartic background.

along the apical direction in Sr$_2$YIrO$_6$, with distinct Ir-O bond lengths 1.9366 (apical), 1.9798, and 1.9723 Å. However, the octahedra in Sr$_2$GdIrO$_6$ are almost undistorted [29]. The lack of momentum dependence of the inelastic features and the fact that we observe almost the same peak positions in these two systems suggest that the electronic structure is determined by local physics such as λ and J_H and is unaffected by the global symmetry or the presence of a small distortion.

In contrast to the Ir DPs, the spectral features in the Re DPs are much broader, partly because of coarser energy resolution. In addition, metallic samples are expected to exhibit large peak width resulting from stronger damping due to the particle-hole continuum as well as the powder-averaging effect, as seen for Ba$_2$FeReO$_6$ and Ca$_2$FeReO$_6$. However, for insulating Ba$_2$YReO$_6$, we find three peaks that can be clearly resolved on top of a broad continuum, so we focus on only this rhenate in our analysis below. The low-energy continuum is modeled with a quartic background; as discussed later, we tentatively attribute this background to coupled multiphonon/magnon contributions. To extract peak positions, the low-energy spectrum from 0.15 to 2.5 eV is fitted with three Lorentzians, as shown in Fig. 2(b). From these fits, we extract peak positions 0.49(3), 0.83(4), and 1.85(5) eV. The corresponding FWHM are 0.13(4), 0.22(8), and 0.29(8) eV, respectively.

IV. THEORETICAL MODEL

We next turn to theoretical modeling of our data. We begin by noting that the sharp, momentum-independent, inelastic peaks found in our RIXS measurements suggest that a local Hamiltonian is appropriate for understanding these excitations. Furthermore, the two sets of compounds in our RIXS study are particle-hole conjugates, with the rhenates being at a filling of two electrons while the iridates are at a filling of two holes. While the local atomic interactions are particle-hole symmetric, SOC breaks this symmetry. As a result, projecting to the t_{2g} orbitals, both sets of materials can be described by the same Kanamori Hamiltonian,

$$H_{\rm eff} = -2J_H\vec{S}^2 - \frac{J_H}{2}\vec{L}^2 \pm \lambda(\vec{l}_1\cdot\vec{s}_1 + \vec{l}_2\cdot\vec{s}_2), \qquad (1)$$

where + (−) with the two-hole (two-electron) picture applies for the d^4 (d^2) configuration and $\vec{L}$ and $\vec{S}$ refer to the total orbital and spin angular momenta, respectively, of the two particles. For $J_H \ll \lambda$, the eigenstates are obtained by perturbing around the noninteracting limit which corresponds to occupying the $j_{\rm eff} = 1/2$ and $j_{\rm eff} = 3/2$ multiplets arising from SOC [50]. For large J_H, the eigenstates should be understood as arising from $\vec{S}$ and $\vec{L}$ being locked together by SOC. In either limit, the d^2 (d^4) case exhibits a ground state with $J_{\rm eff} = 2$ ($J_{\rm eff} = 0$). The d^2 vs d^4 difference arises due to the opposite signs of the effective SOC. While we expect J_H and λ to be similar for Ir and Re, we do not demand that they be identical.

To extract λ and J_H, we plot the calculated excitation energies for the two cases (Ir and Re) as a function of J_H/λ for different choices of λ, as shown in Fig. 3, and superpose on this the observed peak positions. For the correct choice of λ, the computed curves should intersect *all* the observed peaks at a *common* value of J_H/λ, allowing us to extract both λ *and* J_H/λ.

Figures 3(a)–3(c) show the theoretically computed spectra for the Ir DPs as a function of J_H/λ for increasing values of SOC: $\lambda = 0.39$, 0.42 eV, and 0.45 eV, respectively. We also show in these plots the three experimentally observed modes as thick colored lines (pink), with the width indicating the experimental uncertainty. For $\lambda = 0.39$ eV in Fig. 3(a), we find

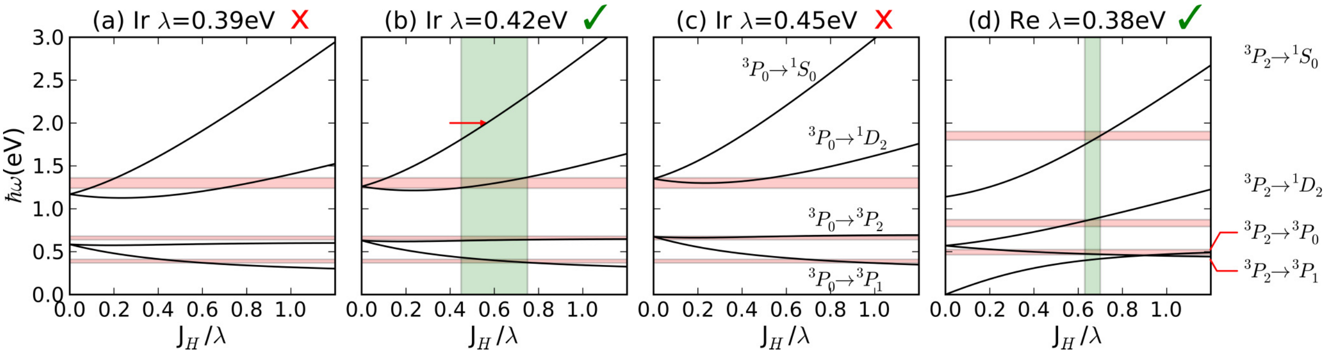

FIG. 3. Calculated excitation energies as a function of J_H/λ are plotted as solid black lines for (a)–(c) Ir and (d) Re double perovskites for indicated λ values. Experimentally determined excitation energies [Ir DP: 0.39(2), 0.66(2), and 1.30(6) eV; Re DP: 0.49(3), 0.83(4), 1.85(5) eV] are plotted as horizontal colored bands (pink), whose widths reflect the experimental uncertainty. States involved in these transitions are labeled using nomenclature in the $J_H \gg \lambda$ limit as ${}^{2S+1}L_J$. (a) and (c) Incorrect and (b) and (d) correct choices of λ as described in the text, which are indicated by × and $\surd$, respectively. Green shaded regions in (b) and (d) illustrate J_H/λ values for which *all* the observed modes intersect the calculated curves. The red arrow in (b) denotes the position of the weak feature ∼2 eV in the Ir-DPs, which would correspond to the highest computed excitation energy.

that the central mode does not intersect the computed spectra for any choice of J_H/λ, while the highest- and lowest-energy modes intersect for $0.65 \lesssim J_H/\lambda \lesssim 0.9$ and $0.45 \lesssim J_H/\lambda \lesssim 0.7$, respectively. For $\lambda = 0.42$ eV in Fig. 3(b), we show that there is a range $0.5 \lesssim J_H/\lambda \lesssim 0.7$, demarcated by the green shaded region, over which *all* observed modes intersect the theoretical curves. Note that Fig. 3(b) also marks the location of the weak ∼2 eV mode with an arrow, showing that this also occurs in the correct regime of J_H/λ; however, given the low intensity of this mode, it should be viewed only as a consistency check. Finally, for even larger SOC, $\lambda = 0.45$ eV in Fig. 3(c), we find that while the central mode intersects the computed spectra over a wide range of J_H/λ, the highest and lowest modes now intersect the theoretical curves for nonoverlapping regimes $J_H/\lambda \lesssim 0.5$ and $0.7 \lesssim J_H/\lambda \lesssim 1.05$, respectively. Thus, there is no single choice of J_H/λ which would explain all the observed modes for the cases in Figs. 3(a) and 3(c), while $\lambda = 0.42$ eV in Fig. 3(b) is a viable choice for the SOC. We show a similar plot for the Re DP in Fig. 3(d) for a choice $\lambda = 0.38$ eV, where we find a small common intersection window near $J_H/\lambda \approx 0.7$. Using this procedure, we conclude that the range of λ values over which such common intersections occur provides an estimate of the SOC, while the window of the common intersection region yields an estimate of J_H/λ. A least-squares fit to the peak positions allows us to determine J_H and λ with remarkably high precision: $\lambda(\mathrm{Ir}) = 0.42(2)$ eV with $J_H(\mathrm{Ir}) = 0.25(4)$ eV and $\lambda(\mathrm{Re}) = 0.38(2)$ eV with $J_H(\mathrm{Re}) = 0.26(2)$ eV. Our result for λ(Ir) is consistent with previous experiments on the single-hole $5d^5$ iridates [51–54]. Further, since Re ($Z = 75$) is close to Ir ($Z = 77$) in the periodic table, we expect similar values for λ and J_H, with a smaller λ for Re given its lower Z, as is borne out by our analysis. Our work highlights the need to treat J_H and λ on equal footing in complex $5d$ oxides.

Interestingly, our model also leads to a simple explanation for why the higher-energy peaks in the RIXS data in the 1–2 eV range (Fig. 2) have much lower spectral weight than the two lower-energy inelastic peaks. As seen from the theoretical plots in Fig. 3, at $J_H/\lambda = 0$, the iridates (rhenates) have two sets of excitations, which correspond to exciting one or two holes (electrons) from $j_{\mathrm{eff}} = 1/2 \to 3/2$ ($j_{\mathrm{eff}} = 3/2 \to 1/2$). These occur at excitation energies $3\lambda/2$ and 3λ, respectively. However, the latter two-particle excitation is not accessed within the RIXS process at $J_H/\lambda = 0$ and thus has *zero* spectral weight. Turning on a small $J_H > 0$ modifies this result in two important ways: (i) it splits these excitations into multiple branches as seen from Fig. 3, and (ii) it leads to a small nonzero spectral weight $\sim(J_H/\lambda)^2$ for the higher-energy peaks from interaction-induced mixing between the $j_{\mathrm{eff}} = 1/2$ and $j_{\mathrm{eff}} = 3/2$ levels. In the next section, we confirm this picture with a theoretical calculation of the RIXS spectrum for the iridate samples.

V. THEORETICAL CALCULATION OF RIXS SPECTRUM

The Kramers-Heisenberg expression for the two-photon scattering cross section is given by

$$\frac{d^2\sigma}{d\Omega dE_i} = \frac{E_o}{E_i}\sum_f \left| \sum_n \frac{\langle f|T^\dagger|n\rangle\langle n|T|g\rangle}{E_g - E_n + E_i + i\frac{\Gamma_n}{2}} \right|^2 \times \delta(E_g - E_f + E_i - E_o). \quad (2)$$

Here, g,n,f refer to initial, intermediate, and final states, respectively, with energies E_g, E_n, E_f, and Γ_n is the inverse lifetime of the intermediate state with a core hole. E_i and E_o are the incoming and outgoing photon energies. The transition is induced by the dipole operator $T \sim \hat{\epsilon}\cdot\mathbf{r}$, where $\hat{\epsilon}$ denotes the photon polarization. Here, we focus on the d^4 iridates at the L_3 resonance within the hole picture, for which the initial and final states come from the two-hole eigenstates on Ir with spin-orbit coupling and Hund's interaction, while the intermediate state corresponds to a single core hole in the atomic $2P_{3/2}$ manifold and a single hole in the $j_{\mathrm{eff}} = 1/2$ manifold. On resonance, with $E_o \approx E_i$ (since the energy transfer is much smaller than the incoming or outgoing photon energies), the cross section

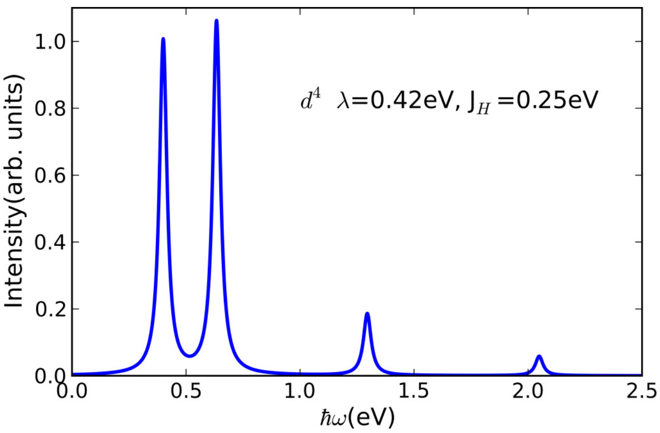

FIG. 4. RIXS spectrum computed for d^4 iridates with $\lambda = 0.42\,\text{eV}$, $J_H = 0.25\,\text{eV}$.

simplifies to

$$\frac{d^2\sigma}{d\Omega dE_i} \approx \left|\frac{1}{E_g - \bar{E}_n + E_i + i\frac{\bar{\Gamma}_n}{2}}\right|^2 \times \sum_f \left|\sum_n \langle f|T^\dagger|n\rangle\langle n|T|g\rangle\right|^2 \times \delta(E_g - E_f + E_i - E_o), \tag{3}$$

where $\bar{E}_n$ and $\bar{\Gamma}_n$ are the average energy and inverse lifetime of the intermediate states, respectively.

We can further simplify the transition matrix element as

$$\langle n|T|g\rangle = \epsilon^{\alpha}_{\text{in}}\langle n|p^{\dagger}_{\beta\sigma} d_{\alpha\beta\sigma}|g\rangle, \tag{4}$$

$$\langle f|T^{\dagger}|n\rangle = \epsilon^{\mu}_{\text{out}}\langle f|d^{\dagger}_{\mu\nu\sigma'} p_{\nu\sigma'}|n\rangle, \tag{5}$$

where we have restricted attention to parity-allowed nonzero dipole matrix elements. Here, $p^{\dagger}_{\alpha\sigma}$ creates a $2P$ core hole in orbital α (i.e., p_x, p_y, p_z) with spin σ, while $d^{\dagger}_{\alpha\beta\sigma}$ creates a d hole in the t_{2g} orbital (i.e., d_{yz}, d_{zx}, d_{xy}) with spin σ. Based on the experimental setup, we fix the incoming polarization to be along the cubic x axis and average the outgoing polarization within the yz plane since the scattering geometry fixes $\hat{\epsilon}_{\text{in}} \cdot \hat{\epsilon}_{\text{out}} = 0$. Using exact diagonalization for the Hilbert space consisting of 15 states for the two-hole problem with the Hamiltonian in Eq. (1) and the single-hole eigenstates of the $2P_{3/2}$ and $j_{\text{eff}} = 1/2$, we obtain the theoretical RIXS spectrum. Figure 4 shows an example of the theoretical spectrum obtained by convolving the above theoretical expression with a Lorentzian resolution function with an experimentally determined width of ~40 meV for a choice of $\lambda = 0.42\,\text{eV}$ and $J_H = 0.25\,\text{eV}$. We find that the two lower-energy peaks have a strong intensity since they emerge from the allowed single-particle transition across the spin-orbit gap $3\lambda/2$, while the two higher-energy peaks have a much lower intensity which scales as $\sim(J_H/\lambda)^2$ for small interactions since they emerge from exciting *two* holes across the spin-orbit gap, which is forbidden in the absence of hole-hole interactions arising from Hund's coupling. The resulting spectral intensities are in good agreement with our experimental results.

VI. DISCUSSION

Despite the excellent agreement between theory and experiments in Fig. 3, there are two unresolved issues. (i) For Re^{5+}, the lowest-energy peak is expected to be at ~0.4 eV. Although this peak is not observed as being distinct from the 0.49 eV peak in our data, it is possible that there are two nearby peaks which are not resolved in our experiment. (ii) For the Re DPs, there is considerable spectral weight in the low-energy continuum below ~0.3 eV. The significant inelastic scattering intensity that was treated as a sloping background in our fitting for Ba$_2$YReO$_6$ [Fig. 2(b)] remains even after subtracting the nonresonant background (see Appendix A). While we can rule out magnon or phonon excitations for energies $\gtrsim$100 meV based on neutron scattering results [55], multiphonon excitations or some collective excitations of coupled degrees of freedom could exist in this energy range. Future measurements with much higher energy resolution could address these issues.

In conclusion, our RIXS experiments on local spin-orbital excitations in Re and Ir double perovskites, together with a well-justified local model Hamiltonian, allow us to reliably extract the SOC $\lambda \sim 0.4\,\text{eV}$ and Hund's coupling $J_H \sim 0.25$ eV for rhenates and iridates. We note that a recent study of the $5d^3$ osmate Ba$_2$YOsO$_6$ reported a smaller $\lambda = 0.32(6)\,\text{eV}$ and a larger $J_H = 0.3(2)\,\text{eV}$ [56]. Although large error bars make these values consistent with our results, it will be interesting to examine whether the discrepancy represents a real difference between d^3 and d^2/d^4 systems. Finally, our results are qualitatively consistent with a $J_{\text{eff}} = 0$ ($J_{\text{eff}} = 2$) for the ground state of the d^4 iridates (d^2 rhenates); however, our finding that $J_H < \lambda$ might require revisiting theories of exotic magnetism in d^2 systems based on a strong-coupling $J_H/\lambda \gg 1$ approach [30].

ACKNOWLEDGMENTS

Research at the University of Toronto was supported by the Natural Sciences and Engineering Research Council of Canada through a Discovery Grant. B.Y. would like to acknowledge support from the Canada Graduate Scholarships-Master's Program. B.C.J. and T.W.N. are supported by the Research Center Program of IBS (Institute for Basic Science) in Korea (IBS-R009-D1). G.C. acknowledges NSF support via Grants No. DMR 1265162 and No. DMR 1712101. This research used resources of the Advanced Photon Source, a U.S. Department of Energy (DOE) Office of Science User Facility operated for the DOE Office of Science by Argonne National Laboratory under Contract No. DE-AC02-06CH11357.

APPENDIX A: BACKGROUND SUBTRACTION

Since intensities of the low-energy resonant inelastic features are greatly reduced for $E_i \gtrsim 11.969\,\text{keV}$, we can use the spectra in this E_i range as a nonresonant background and subtract from our raw data to study the low-energy excitations in Ba$_2$YReO$_6$ [57]. The nonresonant energy spectrum is obtained by summing over the spectra with $E_i = 11.969-11.971$ keV and subtracting from the spectrum at resonant energy ($E_i = 11.961$ keV), as shown in Fig. 5 [57]. The background-subtracted spectrum shown in the inset in Fig. 5 clearly reveals the presence of significant spectral weight

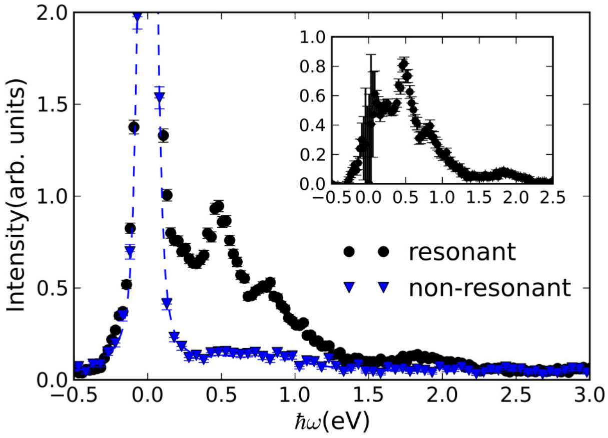

FIG. 5. RIXS spectrum of Ba_2YReO_6 at resonant ($E_i = 11.961$ keV) and nonresonant incident energies (summed from $E_i = 11.969$ keV to $E_i = 11.971$ keV). The spectra have been scaled to have the same intensity at zero-energy transfer. The blue dashed line is fit to the spectrum at nonresonant energy and is used as the background. Inset: Inelastic features obtained by subtracting the background from the resonant spectrum. Clear spectral weight is observed for energy transfer $\hbar\omega < 0.3$ eV.

for $\hbar\omega \lesssim 0.3$ eV. This continuum, which exists in *both* metallic Ba_2FeReO_6 and insulating Ba_2YReO_6, is not captured in our atomic model and will require consideration of multiphonon or other collective excitations.

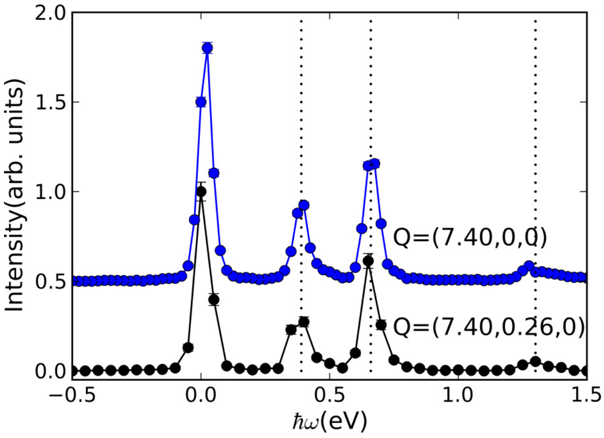

FIG. 6. RIXS spectra of Sr_2YIrO_6 at $\mathbf{Q} = (7.40,0,0)$ and $\mathbf{Q} = (7.40,0.26,0)$. $E_i = 11.215$ keV was used in obtaining both spectra. An arbitrary intensity scale is used, and the spectra are shifted for visual clarity.

APPENDIX B: Sr_2YIrO_6 AND Q DEPENDENCE

We show Sr_2YIrO_6 RIXS spectra measured at two different Q vectors, separated by approximately a quarter of the Brillouin zone, in Fig. 6. The inelastic features remain sharp and show no Q dependence, indicating the local nature of these excitations.

---

[1] O. Kahn and C. J. Martinez, Science **279**, 44 (1998).

[2] R. Heikes, R. Miller, and R. Mazelsky, Physica **30**, 1600 (1964).

[3] S. Yamaguchi, Y. Okimoto, H. Taniguchi, and Y. Tokura, Phys. Rev. B **53**, R2926 (1996).

[4] P. G. Radaelli and S.-W. Cheong, Phys. Rev. B **66**, 094408 (2002).

[5] T. Vogt, P. M. Woodward, P. Karen, B. A. Hunter, P. Henning, and A. R. Moodenbaugh, Phys. Rev. Lett. **84**, 2969 (2000).

[6] L. de' Medici, J. Mravlje, and A. Georges, Phys. Rev. Lett. **107**, 256401 (2011).

[7] W. Z. Hu, J. Dong, G. Li, Z. Li, P. Zheng, G. F. Chen, J. L. Luo, and N. L. Wang, Phys. Rev. Lett. **101**, 257005 (2008).

[8] K. Haule and G. Kotliar, New J. Phys. **11**, 025021 (2009).

[9] M. D. Johannes and I. I. Mazin, Phys. Rev. B **79**, 220510 (2009).

[10] W. L. Yang, A. P. Sorini, C.-C. Chen, B. Moritz, W.-S. Lee, F. Vernay, P. Olalde-Velasco, J. D. Denlinger, B. Delley, J.-H. Chu *et al.*, Phys. Rev. B **80**, 014508 (2009).

[11] S. Zhou and Z. Wang, Phys. Rev. Lett. **105**, 096401 (2010).

[12] N. Raghuvanshi and A. Singh, J. Phys. Condens. Matter **23**, 312201 (2011).

[13] A. A. Schafgans, S. J. Moon, B. C. Pursley, A. D. LaForge, M. M. Qazilbash, A. S. Sefat, D. Mandrus, K. Haule, G. Kotliar, and D. N. Basov, Phys. Rev. Lett. **108**, 147002 (2012).

[14] A. Georges, L. de' Medici, and J. Mravlje, Annu. Rev. Condens. Matter Phys. **4**, 137 (2013).

[15] D. Sutter, C. G. Fatuzzo, S. Moser, M. Kim, R. Fittipaldi, A. Vecchione, V. Granata, Y. Sassa, F. Cossalter, G. Gatti *et al.*, Nat. Commun. **8**, 15176 (2017).

[16] W. Witczak-Krempa, G. Chen, Y. B. Kim, and L. Balents, Annu. Rev. Condens. Matter Phys. **5**, 57 (2014).

[17] I. I. Mazin, H. O. Jeschke, K. Foyevtsova, R. Valentí, and D. I. Khomskii, Phys. Rev. Lett. **109**, 197201 (2012).

[18] K. Foyevtsova, H. O. Jeschke, I. I. Mazin, D. I. Khomskii, and R. Valentí, Phys. Rev. B **88**, 035107 (2013).

[19] Y. Singh and P. Gegenwart, Phys. Rev. B **82**, 064412 (2010).

[20] H. Gretarsson, J. P. Clancy, Y. Singh, P. Gegenwart, J. P. Hill, J. Kim, M. H. Upton, A. H. Said, D. Casa, T. Gog *et al.*, Phys. Rev. B **87**, 220407 (2013).

[21] S. H. Chun, J.-W. Kim, J. Kim, H. Zheng, C. C. Stoumpos, C. D. Malliakas, J. F. Mitchell, K. Mehlawat, Y. Singh, Y. Choi *et al.*, Nat. Phys. **11**, 462 (2015).

[22] B. H. Kim, G. Khaliullin, and B. I. Min, Phys. Rev. B **89**, 081109 (2014).

[23] G. Khaliullin, Phys. Rev. Lett. **111**, 197201 (2013).

[24] A. Akbari and G. Khaliullin, Phys. Rev. B **90**, 035137 (2014).

[25] O. N. Meetei, W. S. Cole, M. Randeria, and N. Trivedi, Phys. Rev. B **91**, 054412 (2015).

[26] C. Svoboda, M. Randeria, and N. Trivedi, Phys. Rev. B **95**, 014409 (2017).

[27] T. Dey, A. Maljuk, D. V. Efremov, O. Kataeva, S. Gass, C. G. F. Blum, F. Steckel, D. Gruner, T. Ritschel, A. U. B. Wolter *et al.*, Phys. Rev. B **93**, 014434 (2016).

[28] S. Bhowal, S. Baidya, I. Dasgupta, and T. Saha-Dasgupta, Phys. Rev. B **92**, 121113 (2015).

[29] G. Cao, T. F. Qi, L. Li, J. Terzic, S. J. Yuan, L. E. DeLong, G. Murthy, and R. K. Kaul, Phys. Rev. Lett. **112**, 056402 (2014).

[30] G. Chen and L. Balents, Phys. Rev. B **84**, 094420 (2011).

[31] S. Calder, J. G. Vale, N. A. Bogdanov, X. Liu, C. Donnerer, M. H. Upton, D. Casa, A. H. Said, M. D. Lumsden, Z. Zhao *et al.*, Nat. Commun. **7**, 11651 (2016).
[32] G. Jackeli and G. Khaliullin, Phys. Rev. Lett. **102**, 017205 (2009).
[33] J. Chaloupka, G. Jackeli, and G. Khaliullin, Phys. Rev. Lett. **105**, 027204 (2010).
[34] Y. Singh, S. Manni, J. Reuther, T. Berlijn, R. Thomale, W. Ku, S. Trebst, and P. Gegenwart, Phys. Rev. Lett. **108**, 127203 (2012).
[35] K. A. Modic, T. E. Smidt, I. Kimchi, N. P. Breznay, A. Biffin, S. Choi, R. D. Johnson, R. Coldea, P. Watkins-Curry, G. T. McCandless *et al.*, Nat. Comm. **5**, 4203 (2014).
[36] T. Takayama, A. Kato, R. Dinnebier, J. Nuss, H. Kono, L. S. I. Veiga, G. Fabbris, D. Haskel, and H. Takagi, Phys. Rev. Lett. **114**, 077202 (2015).
[37] A. Biffin, R. D. Johnson, I. Kimchi, R. Morris, A. Bombardi, J. G. Analytis, A. Vishwanath, and R. Coldea, Phys. Rev. Lett. **113**, 197201 (2014).
[38] J. Knolle, G.-W. Chern, D. L. Kovrizhin, R. Moessner, and N. B. Perkins, Phys. Rev. Lett. **113**, 187201 (2014).
[39] Y. Sizyuk, C. Price, P. Wölfle, and N. B. Perkins, Phys. Rev. B **90**, 155126 (2014).
[40] I. Kimchi, R. Coldea, and A. Vishwanath, Phys. Rev. B **91**, 245134 (2015).
[41] Y. Yamaji, Y. Nomura, M. Kurita, R. Arita, and M. Imada, Phys. Rev. Lett. **113**, 107201 (2014).
[42] K. Pajskr, P. Novák, V. Pokorný, J. Kolorenč, R. Arita, and J. Kuneš, Phys. Rev. B **93**, 035129 (2016).
[43] K. Oikawa, T. Kamiyama, H. Kato, and Y. Tokura, J. Phys. Soc. Jpn. **72**, 1411 (2003).
[44] H. Kato, T. Okuda, Y. Okimoto, Y. Tomioka, K. Oikawa, T. Kamiyama, and Y. Tokura, Phys. Rev. B **69**, 184412 (2004).
[45] B. C. Jeon, C. H. Kim, S. J. Moon, W. S. Choi, H. Jeong, Y. S. Lee, J. Yu, C. J. Won, J. H. Jung, N. Hur *et al.*, J. Phys. Condens. Matter **22**, 345602 (2010).
[46] W. Prellier, V. Smolyaninova, A. Biswas, C. Galley, R. L. Greene, K. Ramesha, and J. Gopalakrishnan, J. Phys. Condens. Matter **12**, 965 (2000).
[47] T. Aharen, J. E. Greedan, C. A. Bridges, A. A. Aczel, J. Rodriguez, G. MacDougall, G. M. Luke, V. K. Michaelis, S. Kroeker, C. R. Wiebe *et al.*, Phys. Rev. B **81**, 064436 (2010).
[48] N. Smolentsev, M. Sikora, A. V. Soldatov, K. O. Kvashnina, and P. Glatzel, Phys. Rev. B **84**, 235113 (2011).
[49] K. Ishii, I. Jarrige, M. Yoshida, K. Ikeuchi, J. Mizuki, K. Ohashi, T. Takayama, J. Matsuno, and H. Takagi, Phys. Rev. B **83**, 115121 (2011).
[50] We use lowercase j_{eff} to denote single-particle (-hole) states, while uppercase J_{eff} is used for the total angular momentum of an ion.
[51] X. Liu, V. M. Katukuri, L. Hozoi, W.-G. Yin, M. P. M. Dean, M. H. Upton, J. Kim, D. Casa, A. Said, T. Gog *et al.*, Phys. Rev. Lett. **109**, 157401 (2012).
[52] L. Hozoi, H. Gretarsson, J. P. Clancy, B.-G. Jeon, B. Lee, K. H. Kim, V. Yushankhai, P. Fulde, D. Casa, T. Gog *et al.*, Phys. Rev. B **89**, 115111 (2014).
[53] M. Moretti Sala, K. Ohgushi, A. Al-Zein, Y. Hirata, G. Monaco, and M. Krisch, Phys. Rev. Lett. **112**, 176402 (2014).
[54] M. Moretti Sala, M. Rossi, S. Boseggia, J. Akimitsu, N. B. Brookes, M. Isobe, M. Minola, H. Okabe, H. M. Rønnow, L. Simonelli *et al.*, Phys. Rev. B **89**, 121101 (2014).
[55] K. W. Plumb, A. M. Cook, J. P. Clancy, A. I. Kolesnikov, B. C. Jeon, T. W. Noh, A. Paramekanti, and Y.-J. Kim, Phys. Rev. B **87**, 184412 (2013).
[56] A. E. Taylor, S. Calder, R. Morrow, H. L. Feng, M. H. Upton, M. D. Lumsden, K. Yamaura, P. M. Woodward, and A. D. Christianson, Phys. Rev. Lett. **118**, 207202 (2017).
[57] D. S. Ellis, J. Kim, J. P. Hill, S. Wakimoto, R. J. Birgeneau, Y. Shvyd'ko, D. Casa, T. Gog, K. Ishii, K. Ikeuchi *et al.*, Phys. Rev. B **81**, 085124 (2010).